Method of Intelligent Diagnosis of Covid-19 Based on a Neural Network of Generalized Bell-Shaped Functions and Fuzzy Logic

Eugene Fedorov[a], Jihed Draouil[b], Kostiantyn Rudakov[a], Hamza Alrababah[c], Tetyana Utkina[a] and Ihor Zubko[a]

[a] *Cherkasy State Technological University, Shevchenko blvd., 460, Cherkasy, 18006, Ukraine*
[b] *Kharkiv National University of Radio Electronics, Nauky ave., 14, Kharkiv, 61166, Ukraine*
[c] *University of Sharjah, Sharjah., 27272, UAE*

Abstract

The paper proposes a method for intelligent diagnosis of COVID-19 based on a neural network of generalized bell-shaped functions and fuzzy logic. The study modern lies in the fact that for intelligent diagnosis COVID-19 was well established as a model of an artificial neural network, selected the three evaluation criteria effectiveness of the proposed models and identified the structure and parameters of the proposed second model based on the method of back propagation in batch mode that is focused on the technology of parallel information processing, and fuzzy diagnostic rules that are formed based on the identified model. The author's models and functions for their structural and parametric adaptation make it possible to increase the reliability, accuracy, speed of decision making. The author's method of intelligent diagnostics can be used in COVID-19 in various intelligent systems of medical diagnostics.

Keywords 1

intelligent diagnostics, COVID-19, artificial neural network, fuzzy logic, CUDA technology

1. Introduction

At present, the epidemic COVID-19 s and the short period of time spread rapidly around the world, which had a destroying impact on the welfare and health of people different countries, as well as on the global economy. At 30.05. 2021, approximately 170 million have contracted COVID-19, of which approximately 3.5 million have officially died due to the disease. Fast, accurate and automated diagnosis of COVID-19 is essential for patient care and pandemic control. Although COVID-19 medicine features are known (respiratory symptoms, cough, fever, shortness of pneumatic and breath), but they do not always indicate COVID-19 and may be at ordinary pneumonia, which complicates the diagnosis of the problem.

Currently, COVID-19 diagnostics uses the following methods:

1. The RT-PCR test [1-3] is the standard for the diagnosis of COVID-19. The disadvantages of RT-PCR provides that it is painful, difficult, time consuming, costly, non-automated and insufficiently accurate [4-6].
2. Computed tomography (CT) [7-9] allows to visualize the chest cell (to receive CCT image) and is a quick and simple procedure. Compared to RT-PCR, the image CT less accurate in the ordinary pneumonia case, but more accurate in case COVID-19. The disadvantages of CT include the risk of disease transmission when using a CT scanning device and its high cost [10-12].

IDDM-2021: 4th International Conference on Informatics & Data-Driven Medicine, November 19–21, 2021 Valencia, Spain
EMAIL: y.fedorov@chdtu.edu.ua (E. Fedorov); jiheddraouil@gmail.com (J. Draouil); k.rudakov@chdtu.edu.ua (K. Rudakov); hamza.alrababah@skylineuniversity.ac.ae (H. Alrababah); t.utkina@chdtu.edu.ua (T. Utkina); i.zubko@chdtu.edu.ua (I. Zubko)
ORCID: 0000-0003-3841-7373 (E. Fedorov); 0000-0002-5250-2673 (J. Draouil); 0000-0003-0000-6077 (K. Rudakov); 0000-0002-7463-0596 (H. Alrababah); 0000-0002-6614-4133 (T. Utkina); 0000-0002-3318-3347 (I. Zubko)
© 2021 Copyright for this paper by its authors.
Use permitted under Creative Commons License Attribution 4.0 International (CC BY 4.0).
CEUR Workshop Proceedings (CEUR-WS.org)

CEUR-WS.org/Vol-3038/paper7.pdf

3. Radiography [13-15] allows visualization of the chest cell (receive CXR image) and is fast and simple procedure. Compared to CT, it is much faster and more economical, since it requires less scarce and expensive equipment. The disadvantages of radiography include the inability to differentiate COVID-19 from other types of pneumonia and is less accurate than CT [16, 17].

Currently, intelligent diagnosis of COVID-19 is usually based on deep and shallow machine learning techniques. At the same time, the most popular are artificial neural networks [18].

The artificial neural networks advantages are:

- The adaptation and training networks;
- The ability to recognition of patterns, their generalization, extracting knowledge from data, i.e., knowledge about the entity (parametric model for object) is not required;
- Data parallel processing, which increases computational complexity.

The artificial neural networks disadvantages are:

- The difficulty of determining the artificial network structure, there are no methods for determining the layers count and neurons in its for different applications;
- The difficulty of forming a representative set of pattern;
- High probability of getting the adaptation and learning method into a local extremum;
- Inaccessibility for knowledge accumulated human understanding by the neural network (it is impossible to represent the relationship between input and output in the form of rules), knowledge are distributed among all neural network items in the form of synaptic weight.

In [19], a deep training model was proposed based on a combination of CNN (for feature extraction) and long short-term memory (LSTM) (for classification) using CXR images, which provided a diagnostic probability of 99.4%.

In [20], the Dark Net deep learning model was proposed, which consists of 17 CNN and YOLO. The disadvantage of this method is the limitation of CXR images.

In [21] used SVM with four kinds of cores (linear, polynomial, sigmoidal, radial basis functions) using CXR images, and for extracting features in the used 4 different models CNN: Google Net, ResNet18, ResNet50 and ResNet101. A diagnostic probability of 100% was achieved with 2 classes (with COVID-19 and no disease) and 97.3% with 3 classes (with COVID-19, with common pneumonia and without disease), but the processing rate was low.

In [22], a deep learning model was proposed through a huge set of CXR images. The disadvantage is that the dataset is unbalanced: 358 CXR images with COVID-19 and 13,000 CXR images with common pneumonia and no disease.

In [23,24], a combination of a deep learning model and a simple CNN using CXR and CCT images was proposed, which provided a diagnostic probability of 94.4%. The disadvantage is that the dataset was small.

In [25], a deep learning model COVIDX-Net was proposed, which consists of 7 different CNN models: InceptionV3, VGG19, ResNe tV2, DenseNet121, Inception-ResNet-V2, MobileNetV2, and Xception using CXR images. Moreover, the probability of diagnosis varied from 60% to 90%, i.e. was insufficient.

In [26], an ensemble of classifiers was used (neural network, decision tree, support vector machine (SVM), naive Bayes, k-nearest neighbours) using CXR images, which provided a 98% diagnostic probability. The downside is that the dataset was small.

In [27], deep learning model was proposed based on the use of 3 different CNN models: Inception-ResNetV2, InceptionV3, ResNet50 using CXR images, and the best diagnostic probability was shown by ResNet50 - 98%.

In [28], a shallow CNN was proposed, which provided high accuracy. The disadvantage is that the set of CXR images was small.

Recently, neural networks have been combined with fuzzy inference systems [29].

The advantages of fuzzy inference systems are:

- Presentation of knowledge in the form of rules, easily accessible for human understanding;
- No need for an accurate assessment of variable objects (incomplete and inaccurate data);

The disadvantages of fuzzy inference systems are:

- Inability of their training and adaptation (the parameters of the membership functions cannot be automatically adjusted);

- Inability of parallel processing of information, which increases the computing power.

In [30] has been proposed adaptive neuro-fuzzy inference system (ANFIS), which provided 98.67% probability of diagnosis at high speed training. The disadvantage of the proposed system was the non-automated determination of the number of values of linguistic variables and the number of fuzzy rules.

In this regard, it is relevant to create a method for intelligent diagnosis of COVID-19, which will eliminate these disadvantages.

The aim is to increase the efficiency intelligent diagnostic COVID-19 due to an artificial neural network with generalized bell-shaped function, which is trained by back propagation method allows to automate the process of extraction of knowledge.

To achieve this goal, it is necessary to solve the following tasks:

1. The choice of a method for the formation of diagnostic features.
2. Creation of a mathematical model of a neural network of bell-shaped functions for COVID-19 diagnostics.
3. Selection of criteria for evaluating the effectiveness of a mathematical model of a neural network bell-shaped functions diagnostics COVID-19.
4. Identification of the structure and parameters of a mathematical model of neural network bell-shaped function diagnosis COVID-19 using the method of backpropagation in batch mode.
5. Creating the parallel algorithm identification of structure and parameters of a mathematical model of a neural network bell-shaped function diagnosis COVID-19 using the method of backpropagation in batch mode.
6. Formation of knowledge in the form of fuzzy rules based on the identified mathematical model of the neural network of bell-shaped functions of COVID-19 diagnostics.

2. Formation of diagnostic features CXR image

Formation of diagnostic features CXR image based on the method of gray-level co-occurrence matrix (GLCM), which allows to reduce feature space and performed as follows:

1. To each color image of a set of data is converted into a grey Picture X, i.e. based on matrices, the matrix is calculated in the form

$$R = [r_{l_1 l_2}], G = [g_{l_1 l_2}], B = [b_{l_1 l_2}]$$

$S = [s_{l_1 l_2}]$ in the Y'UV and Y'IQ models,

$$s_{l_1 l_2} = 0.299 r_{l_1 l_2} + 0.587 g_{l_1 l_2} + 0.114 b_{l_1 l_2},\ l_1, l_2 \in \overline{1, L},$$

or in the HDTV model (ITU-R BT.709 standard)

$$s_{l_1 l_2} = 0.2126 r_{l_1 l_2} + 0.7152 g_{l_1 l_2} + 0.0722 b_{l_1 l_2},\ l_1, l_2 \in \overline{1, L},$$

where $r_{l_1 l_2}, g_{l_1 l_2}, b_{l_1 l_2}$ are red, green and blue components of the pixel.

2. Each grey image is used method of gray-level co-occurrence matrix (GLCM). Preparation matrices denotes as

$$\widehat{P}_\phi = [\widehat{p}_{\phi, l_1, l_2}],$$

Wherein l_1, l_2 – the luminance of neighbouring pixels in the image, $l_1, l_2 \in \overline{1, L}$, φ – angular direction between adjacent pixels, $\phi \in \{0, 45, 90, 135\}$.

The location of neighbouring pixels at different angles is shown in the following example (Fig. 1).

The creation of the GLCM matrix is shown in the following example (Fig. 2)

3. The averaged matrix is calculated in the form

$$\breve{P} = [\breve{p}_{l_1, l_2}],\ \breve{p}_{l_1, l_2} = \frac{1}{4} \sum_\phi \widehat{p}_{\phi, l_1, l_2},\ \phi \in \{0, 45, 90, 135\},\ l_1, l_2 \in \overline{1, L},$$

4. The symmetric matrix is calculated in the form

$$\tilde{P} = \breve{P} + \breve{P}^T$$

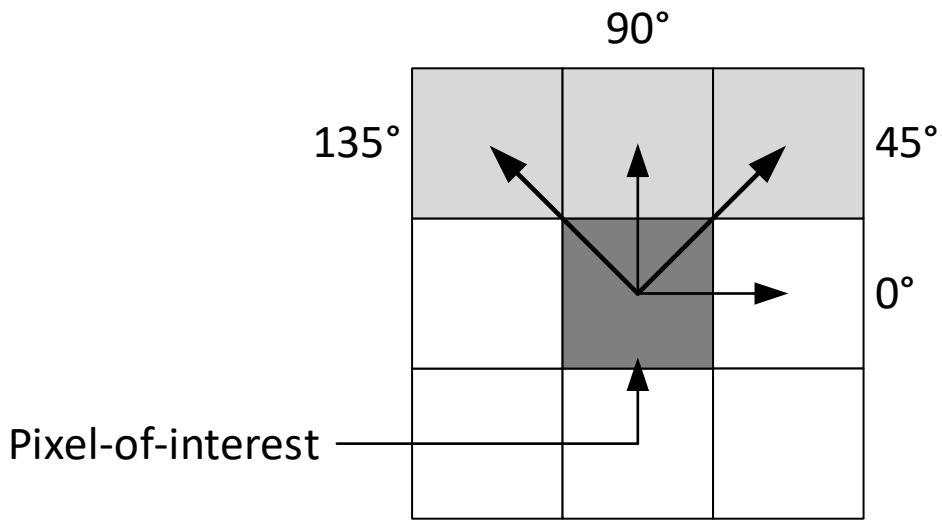

Figure 1: Arrangement of neighbouring pixels at different angles.

5. The matrix is normalized

$$P=[p_{l_1,l_2}],\ p_{l_1,l_2}=\frac{\tilde{p}_{l_1,l_2}}{\sum_{l_1=1}^{L_1}\sum_{l_2=1}^{L_2}\tilde{p}_{l_1,l_2}},\ l_1,l_2\in\overline{1,L}$$

6. The contrast between each pixel and its neighbour is calculated throughout the image.

$$x_1=\sum_{l_1=1}^{L}\sum_{l_2=1}^{L}(l_1-l_2)^2\,p_{l_1,l_2},\ l_1,l_2\in\overline{1,L}$$

1	1	5	6	8
2	3	5	7	1
4	5	7	1	2
8	5	1	2	5

GLCM

	1	2	3	4	5	6	7	8
1	1	2	0	0	1	0	0	0
2	0	0	1	0	1	0	0	0
3	0	0	0	0	1	0	0	0
4	0	0	0	0	1	0	0	0
5	1	0	0	0	0	1	2	0
6	0	0	0	0	0	0	0	1
7	2	0	0	0	0	0	0	0
8	0	0	0	0	1	0	0	0

Figure 2: Arrangement of neighbouring pixels at different angles.

7. Calculating the correlation between the pixel to its neighbour across the image

$$x_2=\frac{\sum_{l_1=1}^{L}\sum_{l_2=1}^{L}(l_1-\mu_{l_1})((l_2-\mu_{l_2})\,p_{l_1,l_2}}{\sigma_{l_1}\sigma_{l_2}},\ l_1,l_2\in\overline{1,L},$$

$$\mu_{l_1}=\sum_{l_1=1}^{L}\sum_{l_2=1}^{L}l_1 p_{l_1,l_2},$$

$$\mu_{l_2} = \sum_{l_1=1}^{L}\sum_{l_2=1}^{L} l_2 p_{l_1,l_2},$$

$$\sigma_{l_1} = \sum_{l_1=1}^{L}\sum_{l_2=1}^{L} (l_1 - (\mu_{l_1})^2) p_{l_1,l_2},$$

$$\sigma_{l_2} = \sum_{l_1=1}^{L}\sum_{l_2=1}^{L} (l_2 - (\mu_{l_2})^2) p_{l_1,l_2}.$$

8. The energy calculated

$$x_3 = \sum_{l_1=1}^{L}\sum_{l_2=1}^{L} \left(p_{l_1,l_2}\right)^2,\ l_1, l_2 \in \overline{1,L}$$

9. Homogeneity is calculated (a elements distribution measure in the normalized matrix to the main diagonal of this matrix)

$$x_4 = \frac{\sum_{l_1=1}^{L}\sum_{l_2=1}^{L} p_{l_1,l_2}}{1+|l_1 - l_2|},\ l_1, l_2 \in \overline{1,L}$$

3. Creating Mathematical models and neural network bell-shaped function diagnostics COVID-19

For the diagnosis of COVID-19, the work has further improved the artificial neural network models through the use of generalized bell-shaped functions (they are a modification of the Cauchy distribution density), which makes it possible to reduce the number of hidden layers, which simplifies the identification of the parameters of the artificial neural network.

The structure of a neural network model of generalized bell-shaped functions (GBFNN) in the graph form is shown in Fig. 3.

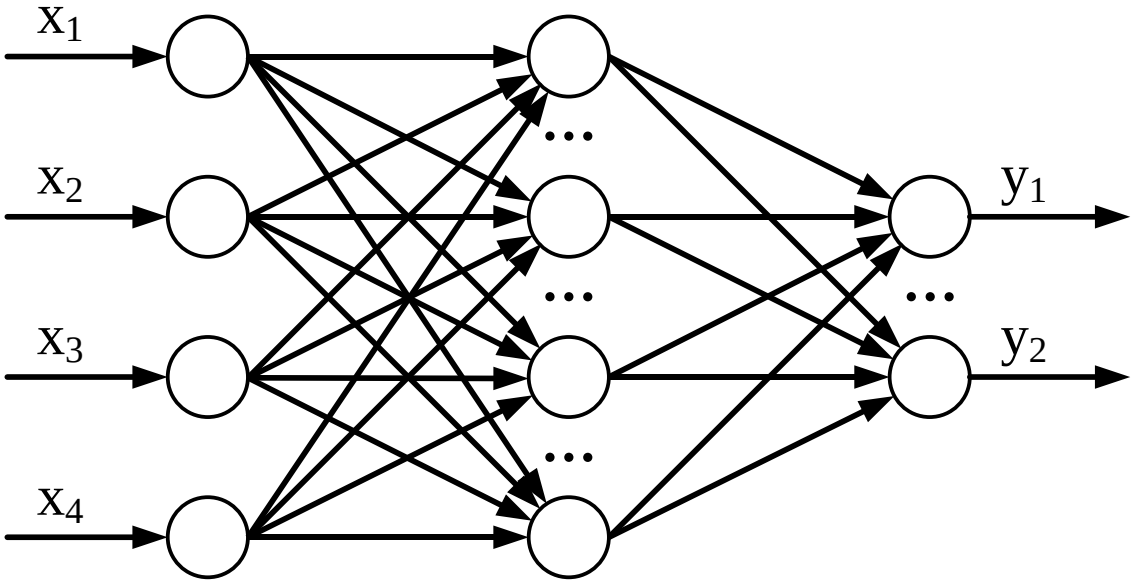

Figure 3: The structure of a neural network model of generalized bell-shaped functions in the graph form.

The input layer with holding $Z = 4$ neurons (neuron corresponding number m the number of input variables). The covered layer contains J neurons (the neurons count corresponds to the fuzzy rules count). The output layer contains $K = 2$ neurons (the number of neurons corresponds to the output variable values count).

The functioning of the neural network of generalized bell-shaped functions is presented as follows.

The hidden layers are calculated multidimensional generalized bell-shaped functions (corresponding to the aggregation of sub-conditions of fuzzy rules, connected in conjunction)

$$y_j^h = f_j(\mathbf{x}) = \prod_{z=1}^{Z} gbell_{zj}(x_z),\ gbell_{zj}(x_z) = \left(1 + \left|\frac{x_z - c_{zj}}{a_{zj}}\right|^{2b_{zj}}\right)^{-1},\ j \in \overline{1, J}.$$

In the output layer, the sums of weighted multidimensional generalized bell-shaped functions are calculated (corresponds to the aggregation of activated fuzzy rules with the same conclusions, i.e. diagnoses)

$$y_k^{out} = \sum_{j=1}^{J} w_{jk} y_j^h,\ k \in \overline{1, K}.$$

Thus, the mathematical model is a neural network generalized bell-shaped functions represented as

$$y_k^{out} = \sum_{j=1}^{J} w_{jk} \prod_{z=1}^{Z} \left(1 + \left|\frac{x_z - c_{zj}}{a_{zj}}\right|^{2b_{zj}}\right)^{-1},\ k \in \overline{1, K}, \quad (1)$$

To decide on the choice of action for the model and (1), the following rule is used

$$k^* = \arg\max_k y_k^{out},\ k \in \overline{1, K}.$$

4. Selection index for evaluating the neural network generalized bell-shaped functions diagnostics COVID-19 model performance

The paper for evaluation of parametric identification of the mathematical model of neural network of generalized bell-shaped functions (1) is selected:

- The criterion of accuracy, which means selection of such parameters $\theta = (a_{11}, ..., a_{ZJ}, b_{11}, ..., b_{ZJ}, c_{11}, ..., c_{ZJ}, w_{11}, ..., w_{JK})$, which deliver a minimum mean square error (the difference output and of the model and the desired outputs)

$$F = \frac{1}{2I} \sum_{i=1}^{I} \sum_{k=1}^{K} (y_{ik}^{out} - d_{ik})^2 \to \min_{\theta}. \quad (2)$$

Where $\mathbf{d}_i = (d_{i1}, ..., d_{iK})$ – i-the test output vector, $d_{ik} \in \{0,1\}$, $\mathbf{y}_i^{out} = (y_{i1}^{out}, ..., y_{iK}^{out})$ – the output vector obtained from the model, I – the number of test implementations.

- The criterion of reliability, that means the selection of such parameters $\theta = (a_{11}, ..., a_{ZJ}, b_{11}, ..., b_{ZJ}, c_{11}, ..., c_{ZJ}, w_{11}, ..., w_{JK})$, which deliver the least probability of making the wrong decision (the difference output and of the model and the desired outputs)

$$F = \frac{1}{I} \sum_{i=1}^{I} \left[\arg\max_{k \in 1,K} y_{ik}^{out} \neq \arg\max_{k \in 1,K} d_{ik} \right] \to \min_{\theta},$$

$$\left[\arg\max_{k \in 1,K} y_{ik}^{out} \neq \arg\max_{k \in 1,K} d_{ik} \right] = \begin{cases} 1, & \arg\max\limits_{k \in 1,K} y_{ik}^{out} \neq \arg\max\limits_{k \in 1,K} d_{ik}, \\ 0, & \arg\max\limits_{k \in 1,K} y_{ik}^{out} = \arg\max\limits_{k \in 1,K} d_{ik}. \end{cases} \quad (3)$$

- The criterion speed, which means selection of such parameters, which deliver the least computational complexity of proposed model

$$F = T \to \min_{\theta}. \quad (4)$$

5. Adaptation of the structure and parameters of a neural network generalized bell-shaped functions diagnosis COVID-19 model based on the method of backpropagation in batch mode

To adaptation the structure and parameters of a neural network generalized bell-shaped functions diagnostics COVID-19 model (1) in the work achieved further improvements in the procedure for determining these parameters based on the method of back propagation and batch training mode to speed up the training, which involves the following steps:

1. Input of training set $\{(\mathbf{x}_i, \mathbf{d}_i) \mid \mathbf{x}_i \in R^Z, \mathbf{d}_i \in \{0,1\}^Z\}, i \in \overline{1, I}$, where $\mathbf{x}_i$ – i-the normalized training input vector, $\mathbf{d}_i$ – i-th training output vector, Z – number of input variables, I – power of the training set. Setting the initial number of neurons in the hidden layer. $J = K$.
2. Iteration number *n = 1*. Initializing by a uniform distribution *U(0, 1)* weights w_{jk}, parameters of activation functions a_{zj}, b_{zj}, c_{zj}, $z \in \overline{1, Z}$, $j \in \overline{1, J}$, $k \in \overline{1, K}$. Iteration number *n = 1*.
3. Calculation of the error energy

$$y_{ik}^{out} = \sum_{j=1}^{J} w_{jk}(n) \prod_{z=1}^{Z} \left(1 + \left| \frac{x_{iz} - c_{zj}(n)}{a_{zj}(n)} \right|^{2b_{zj}(n)} \right)^{-1}, \; i \in \overline{1, I}, \; k \in \overline{1, K}.$$

4. Calculation of the error energy based on criterion (3)

$$E = \frac{1}{2I} \sum_{i=1}^{I} \sum_{k=1}^{K} (y_{ik}^{out} - d_{ik})^2 .$$

5. Setting the weights of the output layer and parameters of the activation functions (backward propagation)

$$w_{jk}(n) = w_{jk}(n) - \eta \frac{\partial E}{\partial w_{jk}(n)}, \; j \in \overline{1, J}, \; k \in \overline{1, K},$$

$$a_{zj}(n+1) = a_{zj}(n) - \eta \frac{\partial E(n)}{\partial a_{zj}(n)}, \; z \in \overline{1, Z}, \; j \in \overline{1, J},$$

$$b_{zj}(n+1) = b_{zj}(n) - \eta \frac{\partial E(n)}{\partial b_{zj}(n)}, \; z \in \overline{1, Z}, \; j \in \overline{1, J},$$

$$c_{zj}(n+1) = c_{zj}(n) - \eta \frac{\partial E(n)}{\partial c_{zj}(n)}, \; z \in \overline{1, Z}, \; j \in \overline{1, J},$$

where η – factor that determines the speed of learning,

$$0 < \eta < 1,$$

$$\frac{\partial E}{\partial w_{jk}} = \frac{1}{I} \sum_{i=1}^{I} f_j(\mathbf{x}_i)(y_{ik}^{out} - d_{ik}),$$

$$\frac{\partial E(n)}{\partial a_{zj}(n)} = \frac{1}{I} \sum_{i=1}^{I} f_j(\mathbf{x}_i) \left(\frac{2b_{zj}}{a_{zj}} \right) \left(1 - gbell_{zj}(x_z)\right) \sum_{k=1}^{K} w_{jk}(n)(y_{ik}^{out} - d_{ik})^2,$$

$$\frac{\partial E(n)}{\partial b_{zj}(n)} = \frac{1}{I} \sum_{i=1}^{I} f_j(\mathbf{x}_i) \left(-2 \ln \left| \frac{x_{zj} - c_{zj}}{a_{zj}} \right| \right) \left(1 - gbell_{zj}(x_z)\right) \sum_{k=1}^{K} w_{jk}(n)(y_{ik}^{out} - d_{ik})^2,$$

$$\frac{\partial E(n)}{\partial c_{zj}(n)} = \frac{1}{I} \sum_{i=1}^{I} f_j(\mathbf{x}_i) \left(\frac{2b_{zj}}{x_{zj} - c_{zj}} \right) \left(1 - gbell_{zj}(x_z)\right) \sum_{k=1}^{K} w_{jk}(n)(y_{ik}^{out} - d_{ik})^2$$

6. Checking the condition for completing the identification of parameters. If $n < N$, then increment n, i.e. *n = n + 1*, go to 3.

7. Checking the condition for completing identification of the structure. If $E > \varepsilon$, then increase the number of neurons in the hidden layer *J*, go to 2. The value is calculated experimentally.
8. Cutting the weights

$$k_j^* = \max\{w_{jk}(n)\},\ j \in \overline{1,J},\ k \in \overline{1,K},$$

$$w_{jk}(n) = (k = k_j^*) w_{jk}(n),\ j \in \overline{1,J},\ k \in \overline{1,K}.$$

6. Parallel algorithm of Identification structure and parameters of a mathematical model of neural network generalized bell-shaped functions diagnosis COVID-19 through the backpropagation method in batch mode

Parallel algorithm of identification structure and parameters of a mathematical model of neural network generalized bell-shaped functions diagnosis COVID-19 through the backpropagation method in batch mode, intended for implementation on GPU via technology CUDA, shown in Fig. 4.

This block diagram functions as follows.

1. Input of training set $\{(\mathbf{x}_i, \mathbf{d}_i) \mid \mathbf{x}_i \in R^Z, \mathbf{d}_i \in \{0,1\}^Z\}, i \in \overline{1,I}$, where $\mathbf{x}_p$ – i-the normalized training input vector, $\mathbf{d}_i$ – i-the teaching output vector, Z – the number of input variables, I – power of the training set. Setting the initial number of neurons in the hidden layer $J = K$.

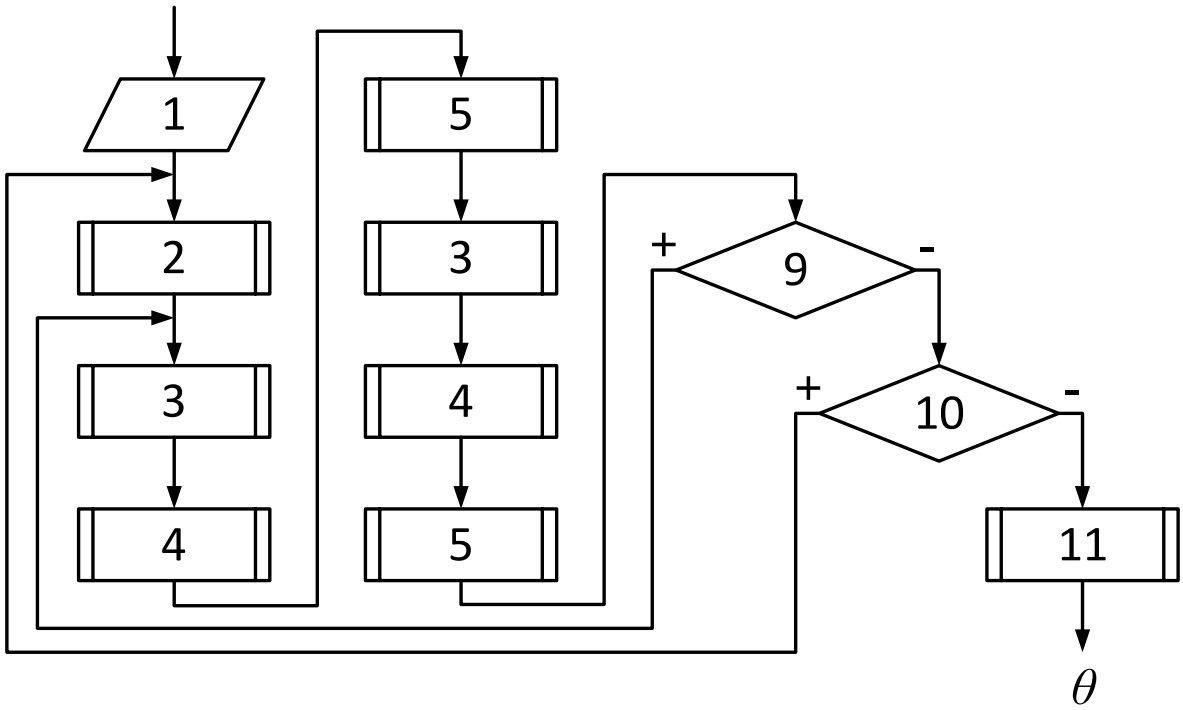

Figure 4: The block diagram of identification of structure and parameters of a mathematical model of neural network generalized bell-shaped functions diagnosis COVID-19 on the basis of the method of backpropagation in batch mode.

2. Iteration number *n = 1*, Initializing by a uniform distribution *U(0, 1)* weights w_{jk}, activation functions parameters

$$a_{zj}, b_{zj}, c_{zj},\ z \in \overline{1,Z},\ j \in \overline{1,J},\ k \in \overline{1,K}.$$

3. Calculation of the output data of layer using KI threads that are grouped into *K* blocks. Each thread computes y_{ik}^{out}.

4. Calculation of the error energy using strands that are grouped into *K* blocks. In each block, on the basis of parallel reduction, a partial sum is calculated from I elements of the form $\frac{(y_{ik}^{out} - d_{ik})^2}{2I}$. The partial amounts received in each block are added up.

5. Adjusting the scales of the output layer w_{jk}, using JKI threads which are grouped into JK blocks. In each block, on the basis of parallel reduction, the sum of I elements of the form is calculated $\frac{1}{I} f_j(\mathbf{x}_i)(y_{ik}^{out} - d_{ik})$.

6. Setting parameters a_{zj}, using ZJI threads which are grouped into ZJ blocks. In each block, on the basis of parallel reduction, the sum of the I elements of the form is calculated $\frac{1}{I} f_j(\mathbf{x}_i)\left(\frac{2b_{zj}}{a_{zj}}\right)\left(1 - gbell_{zj}(x_z)\right)\sum_{k=1}^{K} w_{jk}(n)(y_{ik}^{out} - d_{ik})^2$.

7. Setting parameters b_{zj}, using ZJI threads which are grouped into ZJI blocks. In each block, on the basis of parallel reduction, the sum of I elements of the form is calculated $\frac{1}{I} f_j(\mathbf{x}_i)\left(-2\ln\left|\frac{x_{zj} - c_{zj}}{a_{zj}}\right|\right)\left(1 - gbell_{zj}(x_z)\right)\sum_{k=1}^{K} w_{jk}(n)(y_{ik}^{out} - d_{ik})^2$.

8. Adjusting the parameters c_{zj}, using ZJI threads which are grouped into ZJ blocks. In each block, based on parallel reduction, the sum of the I elements of the form is calculated $\frac{1}{I} f_j(\mathbf{x}_i)\left(\frac{2b_{zj}}{x_{zj} - c_{zj}}\right)\left(1 - gbell_{zj}(x_z)\right)\sum_{k=1}^{K} w_{jk}(n)(y_{ik}^{out} - d_{ik})^2$.

9. Checking the condition for completing the identification of parameters. If $n < N$, then $n = n + 1$, go to 3.

10. Checking the condition for completing identification of the structure. If $E > \varepsilon$, then $J = J + 1$, go to 2.

11. Clipping weights

$$k_j^* = \arg\max\{w_{jk}(n)\},\ j \in \overline{1, J},\ k \in \overline{1, K},$$
$$w_{jk}(n) = (k = k_j^*) w_{jk}(n),\ j \in \overline{1, J},\ k \in \overline{1, K}.$$

7. Formation of knowledge in the form of fuzzy rules based on an identified mathematical model of a neural network of generalized bell-shaped functions of COVID-19 diagnostics

As a result of parametric and structural adaptation on the basis of the trained neural network can generate knowledge, which is represented by fuzzy rules as

R^j : IF $\tilde{x}_1$ there $\tilde{\alpha}_{1j}$ and $\tilde{x}_2$ there $\tilde{\alpha}_{2j}$ and $\tilde{x}_3$ there $\tilde{\alpha}_{3j}$ and $\tilde{x}_4$ there $\tilde{\alpha}_{4j}$ is $\tilde{\alpha}_{4j}$ so $\tilde{y}$ is $\tilde{\beta}_{k^*}$ (F^j), $j \in \overline{1, J}$, where F^j – coefficient of fuzzy rules R^j, $F^j = w_{jk^*}$, $k^* = \arg\max\{w_{jk}\}$, $k \in \overline{1, K}$.

The following linguistic input variables $\tilde{x}_z$ were chosen:

- Contrast $\tilde{x}_1$, with values $\tilde{\alpha}_{11}, ..., \tilde{\alpha}_{1J}$, and their ranges in the fuzzy sets form $\tilde{A}_{11} = \{x_1 \mid \mu_{\tilde{A}_{11}}(x_1)\}$, …, $\tilde{A}_{1J} = \{x_1 \mid 1 - \mu_{\tilde{A}_{1J}}(x_1)\}$;

- Correlation $\tilde{x}_2$, with values $\tilde{\alpha}_{21},...,\tilde{\alpha}_{2J}$, and their ranges in the fuzzy sets form $\tilde{A}_{21}=\{x_2 \mid \mu_{\tilde{A}_{21}}(x_2)\}$, …, $\tilde{A}_{2J}=\{x_2 \mid 1-\mu_{\tilde{A}_{2J}}(x_1)\}$;
- Energy $\tilde{x}_3$, with values $\tilde{\alpha}_{31},...,\tilde{\alpha}_{3J}$, and their ranges in the fuzzy sets form $\tilde{A}_{31}=\{x_3 \mid \mu_{\tilde{A}_{31}}(x_3)\}$, …, $\tilde{A}_{3J}=\{x_3 \mid 1-\mu_{\tilde{A}_{3J}}(x_3)\}$;
- Homogeneity $\tilde{x}_4$, with values $\tilde{\alpha}_{41},...,\tilde{\alpha}_{4J}$, and their ranges in the fuzzy sets form $\tilde{A}_{41}=\{x_4 \mid \mu_{\tilde{A}_{41}}(x_4)\}$, …, $\tilde{A}_{4J}=\{x_4 \mid 1-\mu_{\tilde{A}_{4J}}(x_4)\}$.

In this work, membership functions $\mu_{\tilde{A}_{zj}}(x_z)=gbell_{zj}(x_z)$.

As a linguistic output variable $\tilde{y}$ was selected diagnostic result, with their values $\tilde{\beta}_1$, $\tilde{\beta}_2$, $\tilde{\beta}_3$ (corresponding to the presence COVID-19, presence pneumonia absence of disease) in which the ranges are fuzzy sets $\tilde{B}_1=\{y \mid \mu_{\tilde{B}_1}(y)\}$, $\tilde{B}_2=\{y \mid \mu_{\tilde{B}_2}(y)\}$, $\tilde{B}_3=\{y \mid \mu_{\tilde{B}_3}(y)\}$.

In this work, membership functions $\mu_{B_k}(y)=[y=k]=\begin{cases}1, & y=k\\ 0, & y\neq k\end{cases}$.

8. Numerical research

Numerical research of the offered artificial neural network models, multilayer perceptron, neural network radial basis functions held in the package Matlab using the Deep-Learning Toolbox.

Table 1 shows the root mean square errors (RMSE) and computational complexity, the false diagnostic decisions making probabilities, obtained on the basis of data sets COVID-19 chest X-ray [31], COVID-19 database|SIRM [32], COVID-19 image data collection [33], Radiopaedia COVID-19 [34], Mendeley data - augmented COVID-19 X-ray images dataset [35] using an artificial neural network of the type multilayer perceptron (MLP) and a radial basis function neural network (RBFNN) with backpropagation (BP), and the proposed model (1) with backpropagation (BP). At the same time, MLP had 2 hidden layers (input layer and hidden layer contains of 4 neurons) with logistic activation function, RBFNN had one hidden layer of 8 neurons (twice the neurons count in the hidden layer) with Gauss activation function. P – is the training set power, N – is the number of iterations performed.

Table 1
Root mean square error, computational complexity, false diagnostic decisions probability

Parameter identification model and method	RMSE	False diagnostic decisions probability	Computational complexity
MLP with BP with Logistic Activation Function without CUDA	0.50	0.20	*T = PN*
RBFNN with BP with Gaussian activation function without using CUDA	0.40	0.15	*T = PN*
Proposed model with BP in batch mode with generalized bell-shaped activation function using CUDA	**0.07**	**0.05**	***T = N***

According to Table 1, the best results are obtained by the author's model (1) with the BP parameters adaptation.

According to experiments performed, the next conclusions can be done.

The number of neurons in the hidden layer MLP and RBFNN is not automated and is determined empirically, which reduces the classification accuracy and the speed and identification of model parameters.

The generalized bell-shaped activation function is more efficient than the logistic and Gaussian.

The proposed models make it possible to eliminate these disadvantages.

9. Conclusions

1. To decide the problem of augmentation the efficiency of intelligent diagnostics of COVID-19, the corresponding methods of artificial intelligence were investigated. These studies have shown the use of fuzzy logic in combination with artificial neural networks for analysis CXR image is the most effective method in these days.
2. The proposed method for intelligent diagnosis of COVID-19 is based on fuzzy logic and artificial neural networks for analysis CXR image; providing a representation of knowledge about the diagnosis of COVID-19 in the fuzzy rules form that are understandable by a human; reducing the computational complexity, the false decision making probability, the RMSE due to the automatic selection of the artificial neural network model parameters and structure, the use of parallel processing technology to backpropagation in batch mode.
3. The numerical study has found that the proposed method of intelligent diagnosis COVID-19 provides a probability of wrong decisions made 0.05, and the RMSE 0.10.
4. Further study prospects are the application of the proposed method of intelligent diagnostics of COVID-19 for various intelligent systems of medical diagnostics.

10. References

[1] Sheridan, C.: Coronavirus and the race to distribute reliable diagnostics. Nature Biotechnology. 38, 382–384 (2020). doi:10.1038/d41587-020-00002-2.

[2] Lippi, G., Simundic, A.-M., Plebani, M.: Potential Preanalytical and analytical vulnerabilities in the laboratory diagnosis of CORONAVIRUS disease 2019 (COVID-19). Clinical Chemistry and Laboratory Medicine (CCLM). 58, 1070–1076 (2020). doi:10.1515/cclm-2020-0285.

[3] Lippi, G., Plebani, M.: A six-sigma approach for comparing diagnostic errors IN Healthcare—where does laboratory medicine stand? Annals of Translational Medicine. 6, 180–180 (2018). doi:10.21037/atm.2018.04.02.

[4] Oliveira, B.A., Oliveira, L.C., Sabino, E.C., Okay, T.S.: SARS-CoV-2 and the COVID-19 disease: A mini review on diagnostic methods. Revista do Instituto de Medicina Tropical de São Paulo. 62, (2020). doi:10.1590/s1678-9946202062044.

[5] Ai, T., Yang, Z., Hou, H., Zhan, C., Chen, C., Lv, W., Tao, Q., Sun, Z., Xia, L.: Correlation of Chest CT and Rt-pcr testing for Coronavirus DISEASE 2019 (COVID-19) in China: A report of 1014 CASES. Radiology. 296, (2020). doi:10.1148/radiol.2020200642.

[6] Wolach, O., Stone, R.M.: Mixed-phenotype acute leukemia. Current Opinion in Hematology. 24, 139–145 (2017). doi:10.1097/moh.0000000000000322.

[7] Gozes, O., Frid-Adar, M., Greenspan, H., Browning, P.D., Zhang, H., Ji, W., Bernheim, A., Siegel, E.: Rapid AI development cycle for THE Coronavirus (COVID-19) Pandemic: Initial results for automated detection & patient monitoring using deep LEARNING CT image analysis. URL: https://arxiv.org/abs/2003.05037.

[8] Wang, S., Kang, B., Ma, J., Zeng, X., Xiao, M., Guo, J., Cai, M., Yang, J., Li, Y., Meng, X., Xu, B.: A deep learning algorithm using CT images to screen for Corona virus disease (COVID-19). European Radiology. (2021). doi:10.1007/s00330-021-07715-1.

[9] Ng, M.-Y., Lee, E.Y., Yang, J., Yang, F., Li, X., Wang, H., Lui, M.M.-sze, Lo, C.S.-Y., Leung, B., Khong, P.-L., Hui, C.K.-M., Yuen, K.-yung, Kuo, M.D.: Imaging profile of the COVID-19 Infection: Radiologic findings and literature review. Radiology: Cardiothoracic Imaging. 2, (2020). doi:10.1148/ryct.2020200034.

[10] Wang, S., Zha, Y., Li, W., Wu, Q., Li, X., Niu, M., Wang, M., Qiu, X., Li, H., Yu, H., Gong, W., Bai, Y., Li, L., Zhu, Y., Wang, L., Tian, J.: A fully AUTOMATIC deep learning system FOR

COVID-19 diagnostic and prognostic analysis. European Respiratory Journal. 56, 2000775 (2020). doi:10.1183/13993003.00775-2020.
[11] Salehi, S., Abedi, A., Balakrishnan, S., Gholamrezanezhad, A.: Coronavirus disease 2019 (COVID-19): A systematic review of Imaging findings in 919 PATIENTS. American Journal of Roentgenology. 215, 87–93 (2020). doi:10.2214/ajr.20.23034.
[12] Li, J., Long, X., Wang, X., Fang, F., Lv, X., Zhang, D., Sun, Y., Hu, S., Lin, Z., Xiong, N.: Radiology indispensable for TRACKING COVID-19. Diagnostic and Interventional Imaging. 102, 69–75 (2021). doi:10.1016/j.diii.2020.11.008.
[13] Rubin, G.D., Ryerson, C.J., Haramati, L.B., Sverzellati, N., Kanne, J.P., Raoof, S., Schluger, N.W., Volpi, A., Yim, J.-J., Martin, I.B., Anderson, D.J., Kong, C., Altes, T., Bush, A., Desai, S.R., Goldin, onathan, Goo, J.M., Humbert, M., Inoue, Y., Kauczor, H.-U., Luo, F., Mazzone, P.J., Prokop, M., Remy-Jardin, M., Richeldi, L., Schaefer-Prokop, C.M., Tomiyama, N., Wells, A.U., Leung, A.N.: The role of Chest imaging in patient management during the COVID-19 PANDEMIC: A Multinational consensus statement from the Fleischner society. Radiology. 296, 172–180 (2020). doi:10.1148/radiol.2020201365.
[14] Baratella, E., Crivelli, P., Marrocchio, C., Marco Bozzato, A., De Vito, A., Madeddu, G., Saderi, L., Confalonieri, M., Tenaglia, L., Assunta Cova, M.: Severity of lung involvement on chest x-rays in sars-coronavirus-2 infected patients as a possible tool to predict clinical progression: An observational retrospective analysis of the relationship between radiological, clinical, and laboratory data. Jornal Brasileiro de Pneumologia. 46, (2020). doi:10.36416/1806-3756/e20200226.
[15] Amis, E.S., Butler, P.F., Applegate, K.E., Birnbaum, S.B., Brateman, L.F., Hevezi, J.M., Mettler, F.A., Morin, R.L., Pentecost, M.J., Smith, G.G., Strauss, K.J., Zeman, R.K.: American college of Radiology white paper on radiation dose in medicine. Journal of the American College of Radiology. 4, 272–284 (2007). doi:10.1016/j.jacr.2007.03.002.
[16] Tahir, A.M., Chowdhury, M.E., Khandakar, A., Al-Hamouz, S., Abdalla, M., Awadallah, S., Reaz, M.B., Al-Emadi, N.: A systematic approach to the design and characterization of a Smart INSOLE for Detecting VERTICAL ground reaction FORCE (VGRF) in gait analysis. Sensors. 20, 957 (2020). doi:10.3390/s20040957.
[17] Kallianos, K., Mongan, J., Antani, S., Henry, T., Taylor, A., Abuya, J., Kohli, M.: How far have we come? Artificial intelligence for chest radiograph interpretation. Clinical Radiology. 74, 338–345 (2019). doi:10.1016/j.crad.2018.12.015.
[18] Fedorov E., Lukashenko V.., Patrushev V., Lukashenko A., Rudakov K., Mitsenko S.: The method of intelligent image processing based on a three-channel purely convolutional neural network. CEUR Workshop Proceedings. 2255, 336–351 (2018). URL: http://ceur-ws.org/Vol-2255/paper30.pdf
[19] Islam, M.Z., Islam, M.M., Asraf, A.: A combined deep CNN-LSTM network for the detection of novel coronavirus (COVID-19) using x-ray images. Informatics in Medicine Unlocked. 20, 100412 (2020). doi:10.1016/j.imu.2020.100412.
[20] Ozturk, T., Talo, M., Yildirim, E.A., Baloglu, U.B., Yildirim, O., Rajendra Acharya, U.: Automated detection of COVID-19 cases using deep neural networks with x-ray images. Computers in Biology and Medicine. 121, 103792 (2020). doi:10.1016/j.compbiomed.2020.103792.
[21] Novitasari, D. C. R. et al.: Detection of covid-19 chest x-ray using support vector machine and convolutional neural network. Communications in Mathematical Biology and Neuroscience. (2020). doi:10.28919/cmbn/4765.
[22] Gunraj, H., Wang, L., Wong, A.: Covidnet-ct: A tailored deep convolutional neural network design for detection of covid-19 cases from chest ct images. Frontiers in Medicine. 7, (2020). doi:10.3389/fmed.2020.608525.
[23] El Asnaoui, K., Chawki, Y., Idri, A.: Automated methods for detection and classification pneumonia based on x-ray images using deep learning. Studies in Big Data. 257–284 (2021). doi:10.1007/978-3-030-74575-2_14.
[24] Maghdid, H., Asaad, A.T., Ghafoor, K.Z., Sadiq, A.S., Mirjalili, S., Khan, M.K.: Diagnosing COVID-19 pneumonia from x-ray and CT images using deep learning and transfer learning algorithms. Multimodal Image Exploitation and Learning 2021. (2021). doi:10.1117/12.2588672.

[25] Hemdan, E.E.-D., Shouman, M.A., Karar, M.E.: COVIDX-Net: A framework of deep learning classifiers to Diagnose COVID-19 in x-ray images. URL: https://arxiv.org/abs/2003.11055.
[26] Chandra, T.B., Verma, K., Singh, B.K., Jain, D., Netam, S.S.: Coronavirus disease (COVID-19) detection in chest x-ray images Using majority voting based CLASSIFIER ENSEMBLE. Expert Systems with Applications. 165, 113909 (2021). doi:10.1016/j.eswa.2020.113909.
[27] Narin, A., Kaya, C., Pamuk, Z.: Automatic detection of CORONAVIRUS disease (COVID-19) using x-ray images and deep convolutional neural networks. Pattern Analysis and Applications. 24, 1207–1220 (2021). doi:10.1007/s10044-021-00984-y.
[28] Mukherjee, H., Ghosh, S., Dhar, A., Obaidullah, S.M., Santosh, K.C., Roy, K.: Shallow convolutional neural network FOR COVID-19 Outbreak screening Using chest x-rays. Cognitive Computation. (2021). doi:10.1007/s12559-020-09775-9.
[29] Fedorov E., Nechyporenko O.: Dynamic Stock Buffer Management Method Based on Linguistic Constructions. CEUR Workshop Proceedings. 2870, 1742–1753 (2021). URL: http://ceur-ws.org/Vol-2870/paper126.pdf.
[30] Al-ali, A., Elharrouss, O., Qidwai, U., Al-Maaddeed, S.: ANFIS-Net for automatic detection of covid-19. Scientific Reports. 11, (2021). URL: https://www.nature.com/articles/s41598-021-96601-3.
[31] COVID-19 chest X-ray. (2020). URL: https://github.com/agchung.
COVID-19 database | SIRM. (2020). URL: https://www.sirm.org/en/category/articles/covid-19-database.
[32] Cohen, J.P., Morrison, P., Dao, L.: COVID-19 image data collection, URL: https://export.arxiv.org/abs/2003.11597.
[33] Covid-19. (2020). URL: https://radiopaedia.org/.
[34] Alqudah, A.M.: Augmented covid-19 x-ray images dataset. (2020). URL: https://data.mendeley.com/datasets/2fxz4px6d8/4.